

DISKS AND OUTFLOWS IN THE MASSIVE PROTOBINARY SYSTEM W3(OH)TW

LUIS A. ZAPATA¹, CAROLINA RODRÍGUEZ-GARZA¹, LUIS F. RODRÍGUEZ¹, JOSEP M. GIRART², AND HUEI-RU, CHEN³

To appear in the ApJL.

ABSTRACT

Sensitive and high angular resolution ($\sim 0''.7$) (sub)millimeter line and continuum observations of the massive star forming region W3(OH) made with the Submillimeter Array are presented. We report the first detection of two bipolar outflows emanating from the young and massive "Turner-Welch" [TW] protobinary system detected by the emission of the carbon monoxide. The outflows are massive ($10 M_{\odot}$), highly-collimated (10°), and seem to be the extended molecular component of the strong radio jets and a 22 GHz maser water outflow energized also by the stars in the W3(OH)TW system. Observations of the 890 μm continuum emission and the thermal emission of the CH₃OH might suggest the presence of two rotating circumstellar disk-like structures associated with the binary system. The disks-like structures have sizes of about 1500 AU, masses of a few M_{\odot} and appear to energize the molecular outflows and radio jets. We estimate that the young stars feeding the outflows and that are surrounded by the massive disk-like structures maybe are B-type.

Subject headings: stars: formation — ISM: jets and outflows — ISM: individual objects (W3(OH), W3(H₂O), W3(OH)TW)

1. INTRODUCTION

There is recent observational evidence that the formation of massive stars (early B-type to late O-type) takes place in a way similar to that of solar-type objects, namely by accretion via a circumstellar disk: a handful of cases where a disk could be present around a forming massive star have been presented in the literature (e.g. Fernández-López et al. 2011a,b; Galván-Madrid et al. 2010; Rodríguez et al. 2007; Schreyer et al. 2006; Patel et al. 2005; Shepherd & Kurtz 1999). These disks are larger than those found in forming solar stars and have dimensions of less than 1000 AU and masses of a few solar masses. For more massive stars (i.e. early O-type), the disks appear to be much more massive and larger (e.g. Zapata et al. 2010a; Qiu et al. 2009; Franco-Hernández et al. 2009)

One of the nearest and best-studied sites of ongoing massive star formation is the W3(OH) region. It is located at 2.04 kpc (Hachisuka et al. 2006). Within the W3(OH) region there are clearly two objects that host young massive stars, W3(OH) itself and the Turner-Welch" [TW] object, both bright at radio and millimeter wavelengths (Turner & Welch 1984). W3(OH) is a well-known ultracompact H II region ionized by young OB stars, and rich in OH maser emission (Reid et al. 1995; Wilner et al. 1999; Fish & Sjouwerman 2007). W3(OH)TW or W3(H₂O), on the other hand, seems to be in a younger state, with no associated HII region and with strong dust and molecular emission at (sub)millimeter wavelengths (Wilner et al. 1995; Wyrowski et al. 1997). Bally & Lada (1983) reported faint wings in the CO (J=1-0) spectrum of W3(OH) extending over $\sim 26 \text{ km s}^{-1}$. However, no additional studies for high velocity gas were reported in the literature.

High angular radio observations resolved W3(OH)TW into a binary system: W3(OH)TW-A and W3(OH)TW-C. The spectrum of W3(OH)TW-A from 1.6 to 15 GHz exhibits a power law with spectral index -0.6 and the radio emission has a large elongation in the east-west orientation suggesting

that this object is a synchrotron jet (Reid et al. 1995; Wilner et al. 1999). The elongated continuum source is further coincident, within 0.1 arcsec, with the center of expansion of the H₂O masers and is aligned with the dominant H₂O outflow pattern (Alcolea et al. 1993). At millimeter wavelengths this object shows optically thin dust emission with a spectral index of +3.0 and hot molecular core activity (Chen et al. 2006; Wyrowski et al. 1997). W3(OH)TW-C at radio wavelengths shows a positive spectrum (+0.9), perhaps associated with a thermal radio jet (Wilner et al. 1999). At millimeter wavelengths this source is compact and with positive and steep spectrum (+3.0) related also with optically thin dust emission (Chen et al. 2006; Wyrowski et al. 1997). Additionally, Wyrowski et al. (1997) reported at millimeter wavelengths a third source associated with this zone called W3(OH)TW-B.

2. OBSERVATIONS

2.1. Millimeter

The observations were made with 8 antennas of the SMA⁴ on 2007 August in its compact configuration. The phase reference center for the observations was at R.A. = 02h27m04.30s, decl. = +61°52'24.5" (J2000.0). The frequency was centered at 220.730 GHz in the Lower Sideband (LSB), while the Upper Sideband (USB) was centered at 230.730 GHz. The primary beam of the SMA at around 230 GHz has a FWHM of about 60". The emission from the whole of the W3(OH) region falls very well inside of our FWHM.

The SMA digital correlator was configured in 24 spectral windows ("chunks") of 104 MHz each, with 128 channels distributed over each spectral window, providing a resolution of 0.812 MHz ($\sim 1 \text{ km s}^{-1}$) per channel.

The zenith opacity ($\tau_{230\text{GHz}}$), measured with the NRAO tipping radiometer located at the Caltech Submillimeter Observatory, was from 0.24 to 0.32, indicating reasonable weather conditions during the observations. Observations of Uranus provided the absolute scale for the flux density calibra-

¹ Centro de Radioastronomía y Astrofísica, Universidad Nacional Autónoma de México, Morelia 58090, México

² Institut de Ciències de l'Espai (CSIC-IEEC), Campus UAB, Facultat de Ciències, Torre C5-parell 2, 08193 Bellaterra, Catalunya, Spain

³ Department of Physics, National Tsing Hua University, Hsinchu, Taiwan

⁴ The Submillimeter Array (SMA) is a joint project between the Smithsonian Astrophysical Observatory and the Academia Sinica Institute of Astronomy and Astrophysics, and is funded by the Smithsonian Institution and the Academia Sinica.

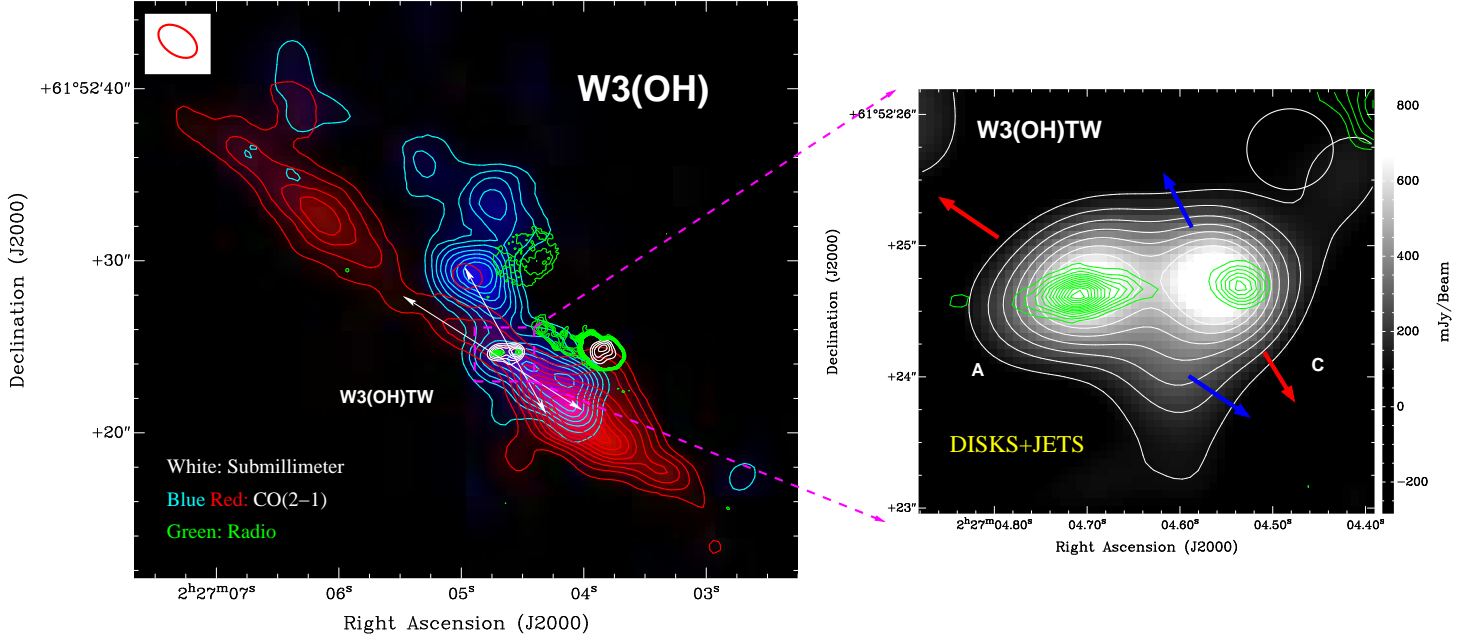


FIG. 1.— LEFT: Integrated intensity color and contour maps of the $^{12}\text{CO}(2-1)$ emission from the W3(OH) region overlaid in contours with the SMA $890\ \mu\text{m}$ continuum emission (white) and the VLA $3.6\ \text{cm}$ continuum emission (green). The blue and red contours are from 30% to 90% with steps of 7% of the peak of the line emission; the peak the $^{12}\text{CO}(2-1)$ emission is $100\ \text{Jy Beam}^{-1}\ \text{km s}^{-1}$. The white contours are from -30% to 90% with steps of 7% of the peak of the emission; the peak of the $890\ \mu\text{m}$ map is $830\ \text{mJy Beam}^{-1}$. The green contours are from 0.45% to 10% with steps of 0.1% of the peak of the emission; the peak at $3.6\ \text{cm}$ is $23\ \text{mJy Beam}^{-1}$. The synthesized beams of the CO and $890\ \mu\text{m}$ continuum are described in the text and are shown in the left and right upper corners of the two images, respectively. RIGHT: A zoom into the W3(OH)TW region. The green and white contours are the same as in the left Figure. The grey scale image shows the SMA $890\ \mu\text{m}$ continuum emission. The color-scale bar on the right indicates the flux scale in mJy. The blue and red arrows represent the position and orientation of the molecular outflows emanating from the massive protobinary.

tion. The gain calibrators were the quasars 0102+584 and 0359+509. The uncertainty in the flux scale is estimated to be between 15 and 20%, based on the SMA monitoring of quasars. Further technical descriptions of the SMA and its calibration schemes can be found in Ho et al. (2004).

The data were calibrated using the IDL superset MIR, originally developed for the OVRO (Scoville et al. 1993) and adapted for the SMA.⁵ The calibrated data were imaged and analyzed in the standard manner using the MIRIAD and KARMA softwares. We set the ROBUST parameter of the task INVERT to -2 to obtain a slightly better resolution sacrificing some sensitivity. The resulting rms noise for the line images was around $200\ \text{mJy beam}^{-1}$ for each velocity channel at an angular resolution of $2''.45 \times 1''.55$ with a P.A. = 65.4° .

2.2. Submillimeter

The observations were made with 7 antennas of the SMA on 2007 August in its extended configuration. The receivers were tuned to a frequency of $346.383\ \text{GHz}$ in the USB, while the LSB was centered on $336.383\ \text{GHz}$. The phase reference center for the observation was R.A. = $02\text{h}27\text{m}03.87\text{s}$, decl. = $+61^\circ52'24.5''$ (J2000.0).

The zenith opacity ($\tau_{230\text{GHz}}$) was from 0.06 to 0.08, indicating excellent weather conditions. Observations of 3C273 with an adopted flux of $8.8\ \text{Jy}$, provided the absolute scale for the flux density calibration. The gain calibrators were the quasars 3C84 and 3C111. For the continuum, we set the ROBUST parameter to -2 to obtain a slightly better resolution sacrificing some sensitivity, while for the line, we use ROBUST = $+2$ to obtain a better signal-to-noise ratio. The continuum and line

images rms noises were around $50\ \text{mJy beam}^{-1}$ and $150\ \text{mJy beam}^{-1}$, respectively at an angular resolution of $0''.74 \times 0''.73$ with a P.A. = 32.7° for the continuum and $0.88'' \times 0.74''$ with a P.A. of 80.4° for the line.

3. RESULTS

3.1. Molecular outflows

In our 2 GHz upper side band of the millimeter observations, we detected the line $^{12}\text{CO}(2-1)$ at a rest frequency of $230.53800\ \text{GHz}$. In Figure 1, we present a map of the integrated intensity over velocity (moment 0) of the line emission observed toward W3(OH). This map was additionally overlaid with the $890\ \mu\text{m}$ continuum emission obtained from these observations and the $3.6\ \text{cm}$ radio emission from Reid et al. (1995), and Wilner et al. (1999). The velocity integration is over the velocity ranges: -75 to $-55\ \text{km s}^{-1}$ (blue) and -45 to $-25\ \text{km s}^{-1}$ (red). The emission at ambient velocities (-54 to $-46\ \text{km s}^{-1}$) was clearly extended and poorly sampled with the SMA, and was suppressed in this moment zero map. This map reveals two strong collimated and bipolar outflows emanating from the massive protobinary system W3(OH)TW, both with similar orientations. One of the bipolar outflows emanates from W3(OH)TW-A with its blueshifted side towards the southwest while its redshifted side is located to the northeast. This outflow has a position angle of $+40^\circ$. The second outflow emanates from W3(OH)TW-C with its blueshifted side towards the northeast while its redshifted side is located to the southwest. This outflow has a position angle of $+15^\circ$. Both outflows show collimation factors of about 10° . The extension of the outflows is about $0.1\ \text{pc}$.

We note that both red lobes appear to be significantly larger than the blue lobes. We tentatively suggest that this effect could be created if very dense molecular material is present

⁵ The MIR-IDL cookbook by C. Qi can be found at <http://cfa-www.harvard.edu/~cqj/mircook.html>

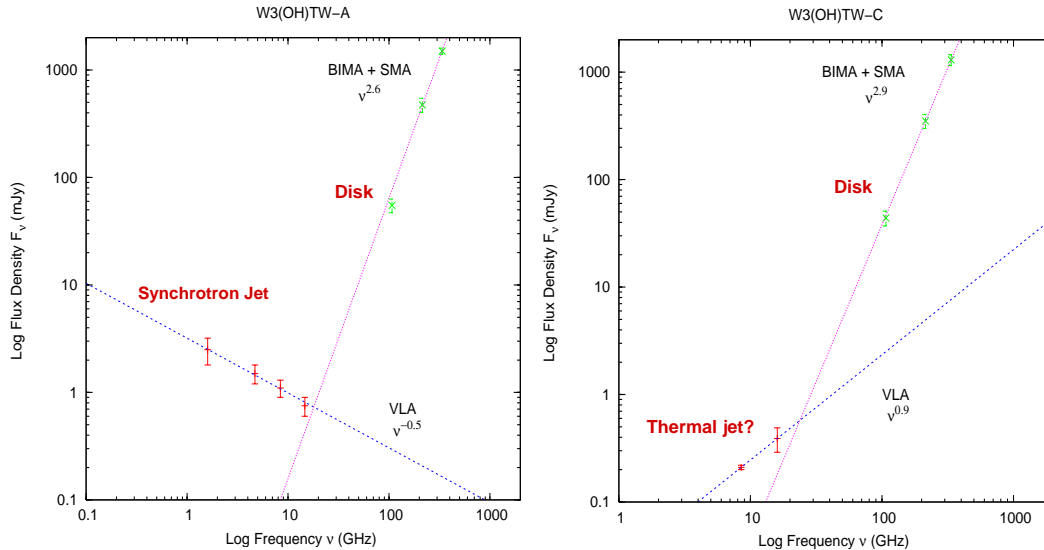


FIG. 2.— Energy spectral distributions for W3(OH)TW-A (left) and W3(OH)TW-C (right) from radio to (sub)millimeter wavelengths. The radio and millimeter data were obtained from Reid et al. (1995), Wilner et al. (1999), and Chen et al. (2006). The submillimeter data is presented here (Table 1). The line is a least-squares power-law fit (of the form $S_\nu \propto \nu^\alpha$) to the spectrum. The α -values of the fitting for the different components of the spectrum are shown in the panels.

between us and the source and that this gas is stopping the development of the blue lobes.

Assuming that we are in local thermodynamic equilibrium (LTE), the molecular emission is optically thin, an excitation temperature equal 50 K, and an abundance ratio of $^{12}\text{CO}/\text{H}_2$ equal to 1×10^{-4} , we can estimate the mass of the outflows for the ^{12}CO molecule in the transition $\Delta J = 2 - 1$. We obtained a mass of about $10 M_\odot$ for each outflow.

For a mechanical force of $F_M = 10 M_\odot 20 \text{ km s}^{-1}/9000 \text{ yr} = 0.03 M_\odot \text{ km s}^{-1} \text{ yr}^{-1}$ and from the correlation presented in Wu et al. (2004) for the outflow mechanical force versus the bolometric luminosity of the exciting source, we very roughly estimate a luminosity for the central powering source on the order of $10^{3-4} L_\odot$, which corresponds to a massive B-type protostar. This spectral type for the central star is in good agreement with that obtained from the dynamical considerations, as we will see in the next section.

It is interesting to note that the molecular outflows are very likely be the extended molecular component of the outflows traced at smaller scales by the radio jets and 22 GHz maser water outflow reported by Reid et al. (1995), Wilner et al. (1999), and Alcolea et al. (1993). However, for example the radio jet associated with the object W3(OH)TW-A has an east-west orientation or a P.A. of $+90^\circ$, while the molecular outflow related with this source has a different orientation toward the southwest-northeast or a P.A. of $+40^\circ$. The 22 GHz maser water outflow has a similar orientation to the radio jet. This might be explained if the ejected material from W3(OH)TW-A bends sometime after the ejection or maybe this source precesses as expected from a binary source. There are some cases where the molecular outflow changes orientation or even precesses, see for example Choi et al. (2006), Zapata et al. (2010b), and Cunningham et al. (2009). Maybe the outflows are arising from different very compact sources within W3(OH)TW-A or perhaps this source could be energizing both outflows as this may precess.

Argon et al. (2003) found several OH masers that are associated with the bipolar outflow traced by the strong H_2O

masers. These OH masers trace the outflow at distances of 1-2'' from the TW-A source, a factor of 2 larger than the distances traced by the water masers. Interestingly, the OH masers suggest that the outflow may be starting to bend in the direction traced by the CO at scales of 5-10''.

3.2. Circumstellar disks?

3.2.1. Continuum emission

In Figure 1, we show the resulting submillimeter ($\lambda = 890 \mu\text{m}$) continuum image obtained with the Submillimeter Array from the high-mass star forming region W3(OH). We detected continuum emission arising from the ultra-compact HII region W3(OH) itself and the massive protobinary system W3(OH)TW. At these wavelengths, the dominant source is W3(OH)TW. The flux density of W3(OH) is about 1.1 Jy. With our present angular resolution ($\sim 0''.7$), we resolve to W3(OH)TW into only two strong objects, namely W3(OH)TW-A and W3(OH)TW-C, already reported at millimeter wavelengths by Chen et al. (2006), and Wyrowski et al. (1997). However, we do not find strong submillimeter emission (at a level of $4\sigma = 200 \text{ mJy}$) associated with the source W3(OH)TW-B reported by Wyrowski et al. (1997).

W3(OH)TW-A and W3(OH)TW-C are well resolved at these wavelengths and show sizes of about 1500 AU at a distance of 2.04 kpc (Hachisuka et al. 2006). However, both objects show different morphologies, the objects associated with W3(OH)TW-A is very elongated in the northeast-southwest direction (with positional angle equal -70°) and with a size of its mayor axis of about 2000 AU, while its minor axis has 1000 AU. W3(OH)TW-C, on the other hand, does not show this marked elongation, this object instead shows a more roundish morphology, with the size of its minor and mayor axis quite similar (of about 1000 AU) and with a positional angle equal -90° , see Table 1.

In Figure 2, we present the Spectral Energy Distributions (SEDs) for W3(OH)TW-A and -C. The spectrum of both objects shows a "combined" two-regime spectrum, with one component observed at radio wavelengths with a nega-

TABLE 1
PHYSICAL PARAMETERS OF THE CIRCUMSTELLAR DISK-LIKE STRUCTURES

	Position ^a		Total Flux	Deconvolved Angular Size ^b	Spectral Index	Disk	Dyn.
	α (J2000)	δ (J2000)	Density (mJy)			Mass M_{\odot}	Mass M_{\odot}
W3(OH)TW	02 27	+61 52	0.87 mm				
A	04.674	24.72	1500±100	$0''.99 \pm 0''.05 \times 0''.43 \pm 0''.05$; $-70^{\circ} \pm 5^{\circ}$	2.6	3.0	16
C	04.551	24.74	1300±150	$0''.56 \pm 0''.05 \times 0''.47 \pm 0''.05$; $-90^{\circ} \pm 10^{\circ}$	2.9	2.0	6

^aUnits of right ascension are hours, minutes, and seconds and units of declination are degrees, arcminutes, and arcseconds.

^bMajor axis \times minor axis; position angle of major axis. The values were obtained using the task IMFIT of MIRIAD.

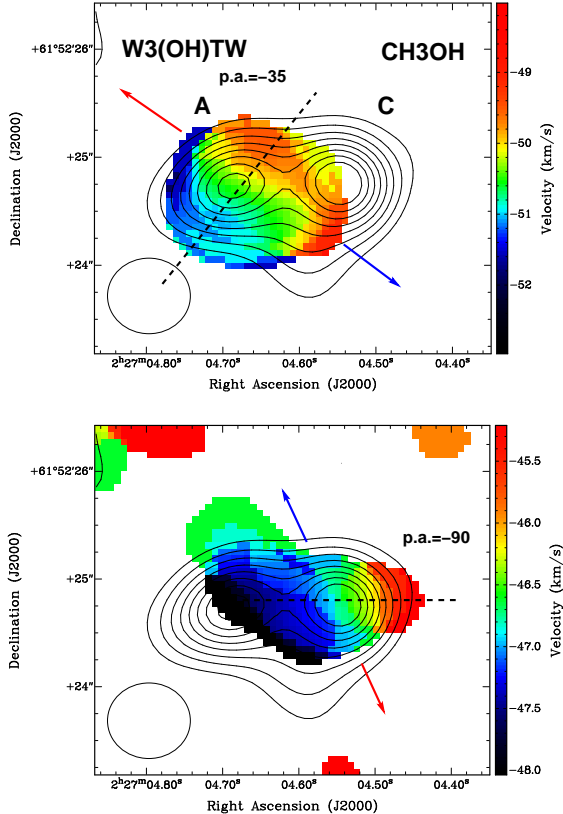


FIG. 3.— UPPER: Integrated intensity weighted velocity map of the CH₃OH[(3,0)-4(2,2)] emission from W3(OH)TW-A overlaid in contours with the 890 μ m continuum emission. The integrated velocity range is from -54 to -46 km s⁻¹. The systemic velocity of W3(OH)TW-A is about -50.5 km s⁻¹. LOWER: Same map as in the upper panel, but now for W3(OH)TW-B. The integrated velocity range is from -42 to -48 km s⁻¹. The systemic velocity of W3(OH)TW-B is about -46.5 km s⁻¹. The color-scale bars on the right indicates the LSR velocities in km s⁻¹. The synthesized beam of the line image is shown in the bottom left corner of each image. The dashed lines in each panel mark the orientation and position were the PV-diagrams presented in Figure 4 were made. The synthesized beam of the images is $0.88'' \times 0.74''$ with a P.A. of 80.4° and is shown in the left corner of the figures.

tive/positive slowly rising spectrum (with $\alpha = -0.5$ for A and $\alpha = 0.9$ for B) and that are related with synchrotron/thermal? jets (Reid et al. 1995; Wilner et al. 1999). The second component is observed at (sub)millimeter wavelengths with the emission that rises rapidly with frequency, and is associated with optically thin dust emission from a circumstellar disk or maybe an envelope (Wyrowski et al. 1997, 1999; Chen et al. 2006).

We have obtained the spectral indices ($S_{\nu} \propto \nu^{\alpha}$) for both structures from the millimeter and submillimeter

BIMA+SMA observations, see Table 1. The spectral indices are very steep (2.6 for the component A and 2.9 for the component B) which are consistent with optically thin dust emission and with a dust mass opacity coefficient that varies with frequency as $\kappa_{\nu} \propto \nu^{0.6-0.9}$. This spectral index determination is reliable since the 0.89, 1.4, and 2.8 mm observations have similar angular resolution ($\leq 1''$) and are in very good agreement with those values obtained at millimeter wavelengths by Chen et al. (2006).

With this information, we can estimate the masses of the 890 μ m sources. Adopting a value of $\kappa_{1.4mm} = 1.5$ cm² g⁻¹ (the average of the values of 1.0 cm² g⁻¹, valid for grains with thick dust mantles, and 2.0 cm² g⁻¹, valid for grains without mantles). This implies $\kappa_{890\mu m} \sim 2.0$ cm² g⁻¹. Assuming optically thin, isothermal dust emission and a gas-to-dust ratio of 100, and a dust temperature of 100 K for the (sub)millimeter objects (Chen et al. 2006), we derive masses of about a few solar masses (see Table 1). These values for the mass are in reasonable agreement with the values found by Chen et al. (2006) for W3(OH)TW-A equal to 5 M_{\odot} and for W3(OH)TW-C equal to 4 M_{\odot} . The differences would be attributed to the observations of Chen et al. (2006) probably are recovering more extended emission from the objects.

The dimensions (~ 1500 AU), the masses (of a few M_{\odot}), and that from both sources emanate at large scales powerful molecular outflows and at small scales thermal/non-thermal jets (Figure 1) suggest that W3(OH)TW-A and -C contain massive circumstellar disks. Furthermore, the two submillimeter objects have orientations consistent with the ejection of the outflows (Table 1).

The derived masses and sizes of the two hypothesized disks (Table 1) will make fairly large optical depths of 0.3 in the dust emission. In such case, the spectral index may be affected by the optical depth and the assumption of optically thin dust emission might be not correct at all.

There is, however, a problem with the interpretation of W3(OH)TW-A being a massive circumstellar disk. The orientation of the synchrotron jet and the H₂O maser outflow that emanates from this source has an east-west orientation, and is not consistent with the orientation of the disk-like structure. However, as mentioned before, maybe W3(OH)TW-A is precessing or the putative disk is actually circumbinary, and one compact source in the middle drives the radio jet, and the second one the molecular outflow.

3.2.2. Line emission

In our 2 GHz lower side band of the submillimeter observations, we detected the line CH₃OH[(3,0)-4(2,2)] $v_t=0,1$ at a rest frequency of 337.135873 GHz. Figure 3 shows maps of the intensity-weighted velocity (moment 1), overlaid with the 890 μ m continuum emission obtained by averaging the line-free channels in our SMA observations. These maps reveal

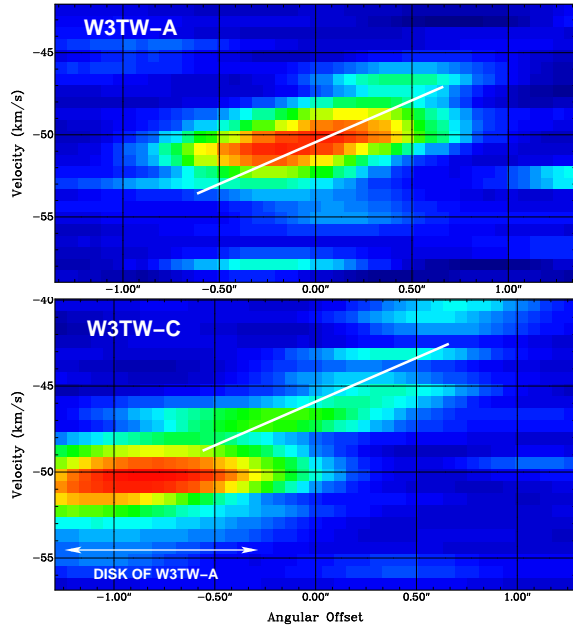


FIG. 4.— Position velocity diagrams computed from Figure 3. UPPER: PV diagram for W3(OH)TW-A. LOWER: PV diagram for W3(OH)TW-B. The units of the vertical axis are in arcseconds. The synthesized beam of the images is $0.88'' \times 0.74''$ with a P.A. of 80.4° . The spectral resolution is 0.704 km s^{-1} . The white lines in the panels mark the velocity gradient found in every circumstellar disk.

compact and strong submillimeter molecular emission arising only from the continuum sources and with clear velocity gradients of a few kilometers per second. W3(OH)TW-A shows a velocity gradient of about $8 \text{ km s}^{-1} \text{ arcsec}^{-1}$ at a position angle of -35° and W3(OH)TW-C of about $6 \text{ km s}^{-1} \text{ arcsec}^{-1}$ at a position angle of -90° . In Figure 3, we only present the strongest CH_3OH emission from both sources, however, in

Figure 4 we show more clearly the full magnitude of the velocity gradients. The systemic velocities of each source are a bit different, we find that W3(OH)TW-A is at -50.5 km s^{-1} , while W3(OH)TW-C is at -46.5 km s^{-1} . Assuming that the two sources are separated by $\sim 1''$ and in a bound circular orbit, we estimate a lower limit of $30 M_\odot$ for the whole system. We note that the orientation of the velocity gradient found in these objects are in very good agreement with the position of the mayor axis of the circumstellar disk-like structures (Table 1) suggesting that we are likely seeing the rotation of the molecular gas in them.

In Figure 4, we show the kinematics of the molecular gas of both possible circumstellar disks. In the position-velocity diagrams it is much more clear to see the gradients and their magnitudes. The velocity gradients are clearly linear and associated with the rotation of a rigid body. However, to detect the Keplerian motions, typically observed in many low-mass circumstellar disks, we need much more angular and spectral resolution. Zapata et al. (2010a) noted that the Keplerian motions of the extremely large circumstellar disk associated with the massive young object W51 North are more pronounced close to the protostar while in the edges the molecular gas moves more like a rotating ring. Assuming that the velocity gradients are Keplerian, we find that the dynamical mass for W3(OH)TW-A is $16 M_\odot$ and for W3(OH)TW-C is $6 M_\odot$. The sizes of the line emission are similar to those found in the dust continuum emission. Those values are in good agreement with Chen et al. (2006) that reported a total dynamical mass for the system of about $22 M_\odot$. However, we note that they could not separate the velocity gradient of each disk, they instead reported a single gradient across the system.

Thus, the protostar associated with W3(OH)TW-A has a mass of approximately $13 M_\odot$, while the associated with W3(OH)TW-C has a mass of $4 M_\odot$, which corresponds to B-type stars.

REFERENCES

- Alcolea, J., Menten, K. M., Moran, J. M., & Reid, M. J. 1993, *Astrophysical Masers*, 412, 225
- Argon, A. L., Reid, M. J., & Menten, K. M. 2003, *ApJ*, 593, 925
- Bally, J., & Lada, C. J. 1983, *ApJ*, 265, 824
- Chen, H.-R., Welch, W. J., Wilner, D. J., & Sutton, E. C. 2006, *ApJ*, 639, 975
- Choi, M., Hodapp, K. W., Hayashi, M., Motohara, K., Pak, S., & Pyo, T.-S. 2006, *ApJ*, 646, 1050
- Cunningham, N. J., Moeckel, N., & Bally, J. 2009, *ApJ*, 692, 943
- Franco-Hernández, R., Moran, J. M., Rodríguez, L. F., & Garay, G. 2009, *ApJ*, 701, 974
- Fernández-López, M., Curiel, S., Girart, J. M., Ho, P. T. P., Patel, N., & Gómez, Y. 2011, *AJ*, 141, 72
- Fernández-López, M., Girart, J. M., Curiel, S., Gómez, Y., Ho, P. T. P., Patel, N. 2011, *AJ*, submitted
- Fish, V. L., & Sjouwerman, L. O. 2007, *ApJ*, 668, 331
- Galván-Madrid, R., Zhang, Q., Keto, E., Ho, P. T. P., Zapata, L. A., Rodríguez, L. F., Pineda, J. E., & Vázquez-Semadeni, E. 2010, *ApJ*, 725, 17
- Hachisuka, K., et al. 2006, *ApJ*, 645, 337
- Ho, P. T. P., Moran, J. M., & Lo, K. Y. 2004, *ApJ*, 616, L1
- Qiu, K., Zhang, Q., Wu, J., & Chen, H.-R. 2009, *ApJ*, 696, 66
- Patel, N. A., et al. 2005, *Nature*, 437, 109
- Reid, M. J., Argon, A. L., Masson, C. R., Menten, K. M., & Moran, J. M. 1995, *ApJ*, 443, 238
- Rodríguez, L. F., Zapata, L. A., & Ho, P. T. P. 2007, *ApJ*, 654, L143
- Turner, J. L., & Welch, W. J. 1984, *ApJ*, 287, L81
- Schreyer, K., Semenov, D., Henning, T., & Forbrich, J. 2006, *ApJ*, 637, L129
- Scoville, N. Z., et al. 1993, *PASP*, 105, 1482
- Shepherd, D. S., & Kurtz, S. E. 1999, *ApJ*, 523, 690
- Wilner, D. J., Reid, M. J., & Menten, K. M. 1999, *ApJ*, 513, 775
- Wilner, D. J., Welch, W. J., & Forster, J. R. 1995, *ApJ*, 449, L73
- Wu, Y., Wei, Y., Zhao, M., Shi, Y., Yu, W., Qin, S., & Huang, M. 2004, *A&A*, 426, 503
- Wyrowski, F., Hofner, P., Schilke, P., Walmsley, C. M., Wilner, D. J., & Wink, J. E. 1997, *A&A*, 320, L17
- Wyrowski, F., Schilke, P., Walmsley, C. M., & Menten, K. M. 1999, *ApJ*, 514, L43
- Zapata, L. A., Tang, Y.-W., & Leurini, S. 2010, *ApJ*, 725, 1091
- Zapata, L. A., Schmid-Burgk, J., Muders, D., Schilke, P., Menten, K., & Guesten, R. 2010, *A&A*, 510, A2